Particle-fluid interaction inside a beater mill

2016 J. Phys.: Conf. Ser. 760 012017

(http://iopscience.iop.org/1742-6596/760/1/012017)

Particle-fluid interaction inside a beater mill

M J Marijnissen[1] **and J Rojek**[1]

[1]Institute of Fundamental Technological Research, Polish Academy of Sciences, Pawińskiego 5b, 02-106 Warsaw, Poland

E-mail: mmarijn@ippt.pan.pl

Abstract In this work a trajectory study of particles through a beater mill (sometimes referred to as a fan mill) was performed. The attention was focused on particle behaviour. We used the CFD-DEM (Discrete Element Method) commercial code, ANSYS Fluent. Particles of different sizes were analysed. Results highlight particle behaviour, fluid flow conditions and mark places requiring geometrical improvements. Most of the improvements needed are in the mill's classifier, where perpendicular walls and large vortices hinder the filtration process, by suspending the particles inside the classifier.

1. Introduction

We can create a general division in the processes of comminution based on particle velocities. On one side of the scale we can put standard ball mills, with slow velocities. On the other side of the spectrum we can put beater mills. Standard ball mills have been known to take up to 50% of the ore production process's energy requirement [1]. Beater mills on the other hand seem to compete in energy efficiency whilst achieving high internal fluid velocities due to a spinning flywheel with its axis of revolutions normal to the flow. After hitting the flywheel the particles are shed upward into a classifier, where particles small enough are passed further on towards the next process. Particles considered too big are recirculated back onto the flywheel. Particle-fluid interaction plays a grand role in high speed comminution. Any improvements made into this process have an immense impact on cost reduction. The analysis of particle trajectories allows for insight in the current design of beater mills and provides ground for further improvements. With high internal flow velocities a particle-fluid coupling is required to simulate the appropriate behaviour of the ore. This was achieved with a CFD-DEM coupling which has been used in simulations and validations of particulate flow in a channel [2], fluidized beds [3] and slurry flow [4]. Additionally it has successfully been tested against analytic and experimental data [5].

2. Model description

We considered a multiphase fluid model where the fluid was treated as a continuous phase and the solid phase as discrete particles. The fluid was considered compressible and the flow turbulent. The k-ω turbulence model was used to take account for turbulent flow. Particle volume fraction were taken into consideration during calculations. Mass and heat exchange between phases were omitted. Discrete particles are considered undeformable and their drag coefficient is unaffected by neighbouring particles or compressibility effects. A two-way coupling is used between the continuous and the discrete phase.

2.1. Fluid flow

The Finite Volume Method is used to calculate the fluid taking into consideration of the particle volume fraction in given cells. A multiphase fluid is modelled with the use of conservation equations for a particular phase as given by

$$\frac{\partial \alpha_q \rho_q}{\partial t} + \nabla \cdot (\alpha_q \rho_q \vec{u}_q) = 0 \tag{1}$$

$$\frac{\partial \alpha_q \rho_q \vec{u}_q}{\partial t} + \nabla \cdot (\alpha_q \rho_q \vec{u}_q \vec{u}_q) = \alpha_q \rho_q \vec{g} - \alpha_q \nabla p_r + \nabla \cdot \bar{\tau}_q + \vec{F}_{add,q} \tag{2}$$

$$\bar{\tau}_q = \alpha_q \mu_q (\nabla \vec{u}_q + \nabla \vec{u}_q^T) + \alpha_q (\lambda_q - \frac{2}{3}\mu_q) \nabla \cdot \vec{u}_q I \tag{3}$$

$$\frac{\partial h_q \rho_q}{\partial t} + \nabla \cdot (\alpha_q \rho_q \vec{u}_q h_q) = \alpha_q \frac{\partial p_{rq}}{\partial t} + \bar{\tau}_q \cdot \nabla \vec{u}_q - \nabla \cdot \vec{q}_q . \tag{4}$$

In these equations α is the phasic volume fractions, $\vec{u}$ is the velocity of the fluid, g gravity, ρ density, p_r pressure and subscript q denotes the phases respectively. Additionally λ and μ denote the shear and bulk viscosity. Moreover $\bar{\tau}$ is the stress tensor and $\vec{F}_{add}$ represents additional forces (e.g. contact, coupling, pressure gradient) and $\vec{g}$ is the gravitational acceleration. Lastly h is the specific enthalpy and $\vec{q}$ is the heat flux, while t is the time variable. The model presented here holds for a n-phase fluid, while we only used one fluid phase with the volume fractions taken from the discrete phase. Details of the k-ω turbulence model can be found in [6].

2.2. Discrete Element Method

The DEM was first introduced by [7]. Since then the processing power of computers has increased allowing for increasing use of this method. In DEM we track the position of discrete particles in a Lagrangian reference frame as given by

$$\rho_p V_p \frac{d\vec{u}_p}{dt} = \vec{F}_{drag} + \vec{g}(\rho - \rho_p) V_p + \vec{F}_{add.} \tag{5}$$

$$\vec{F}_{drag} = \frac{3\mu C_d \,\mathrm{Re}}{4 d_p^2} \tag{6}$$

$$\mathrm{Re} = \frac{\rho d_p \,|\vec{u} - \vec{u}_p\,|}{\mu} \tag{7}$$

$$C_d = \begin{cases} 0.424 & : \mathrm{Re} > 1000 \\ \dfrac{24}{\mathrm{Re}}\left(1 + \dfrac{\mathrm{Re}^{2/3}}{6}\right) & : \mathrm{Re} \le 1000 \end{cases}. \tag{8}$$

Here equation (5) represents the forces acting upon the particles, where $\vec{u}$ is the fluid velocity, ρ indicates the fluid density, μ the molecular viscosity. V is the particle volume. All variables containing the subscript p consider the particle. Moreover $\vec{F}_{add.}$ represents additional forces acting upon the particle (ex. contact, coupling, pressure gradient) and $\vec{F}_{drag}$ can be described as shown in equations (6) and (7). What remains is the definition of the particle drag coefficient. We did not take into account for other particles shapes than spherical, so we used the formula presented by equation (8) without any shape coefficients.

2.3. Particle contact

Contact between particles is considered. The particles are allowed to overlap for a small distance. This overlap is the deciding factor while calculating the contact force. For the overlap to be small it is crucial to use a small time step. When an overlap is detected contact forces are calculated and applied to the particles. The governing equations are given by

$$\vec{e}_{12} = \frac{x_2 - x_1}{\|x_2 - x_1\|} \tag{9}$$

$$\delta = \|x_2 - x_1\| - (r_2 + r_1) \tag{10}$$

$$\vec{F}_1 = -\vec{F}_2 = (k\delta + \gamma \vec{u}_{12} \cdot \vec{e}_{12})\vec{e}_{12} \tag{11}$$

$$\vec{F}_{\text{tan}\,gential} = \beta(u_r)\vec{F}_{normal}. \tag{12}$$

Where δ is the overlap, x_1 is the coordinate position of the centre of the particle. r_1 and $\vec{F}_1$ its radius and force acting upon the particle. Index 2 refers to the second particle whereas k and γ are the spring and damping coefficients. Finally $\beta(u_r)$ is the tangential friction coefficient dependent on radial velocity.

2.4. Coupling

After a velocity field is obtained the forces are calculated on the DEM particles which change their position accordingly. New particle coordinates as well as forces, are passed back on to the fluid flow part of the simulation. This process creates a 2-way coupling, were the fluid acts upon the particles and likewise, the particles on the fluid. The coupling is achieved by the α and $\vec{F}_{add.}$ variables presented in equation (1)-(5). For stability purposes, it is recommended for the particle time step to be small.

3. Geometry and mesh

The geometry was obtained from the producers of the mill. The gross dimensions of the whole mill are 5.5 m of height, 3 m of depth and 2.5 m of width. The mill's flywheel has a diameter just below 2 m and spins at 1000 RPM. The mesh consists of approximately 600.000 elements and is presented next to the geometry in figure 1. Additionally the inlet surface is marked with a green colour, whilst the outlet surfaces are marked in red. During simulations the angle of the flaps inside the classifier as well as before the flywheel were held constant.

4. Boundary and initial conditions

For the inflow a mass flow inlet boundary condition was used. The mass flow was set to match the parameters given by the producers. On the outlet a pressure-outlet condition was assigned with a -50 Pa pressure recreating the conditions behind the mill. The flywheel and its nearest fluid was set in a rotary frame. A time step of $5 \cdot 10^{-5}$ s was used to insure stability. After the simulation stabilized 360 particles were injected evenly on the inlet. The mass flow inlet of particles was much smaller than intended but was limited to save computational time and to increase the tracking ease of single particles. There were 3 groups of particles injected separately upon simulation conditions stabilized with a diameter of 10^{-6}, 10^{-5} and 10^{-4} m. The density for each particle was set the same at 1550 kg/m^3. Particles were injected with the same velocity as the fluid on the inlet surface, after which the simulation was run for another 0.72 seconds. This procedure was done to ensure no interaction between bigger and smaller particles and to study the behaviour of each size fraction during transition. Particles upon reaching the outlet were deleted from the computational domain. The amount of particles was compared after the same simulation run time. The fluid flow conditions in which the particles were injected are shown in figure 2 with 2 cross-sections and a close up of the classifier. This

close up shows a surprising amount of big vortices and a complicated flow pattern. These conditions pose a problem for particle size filtration.

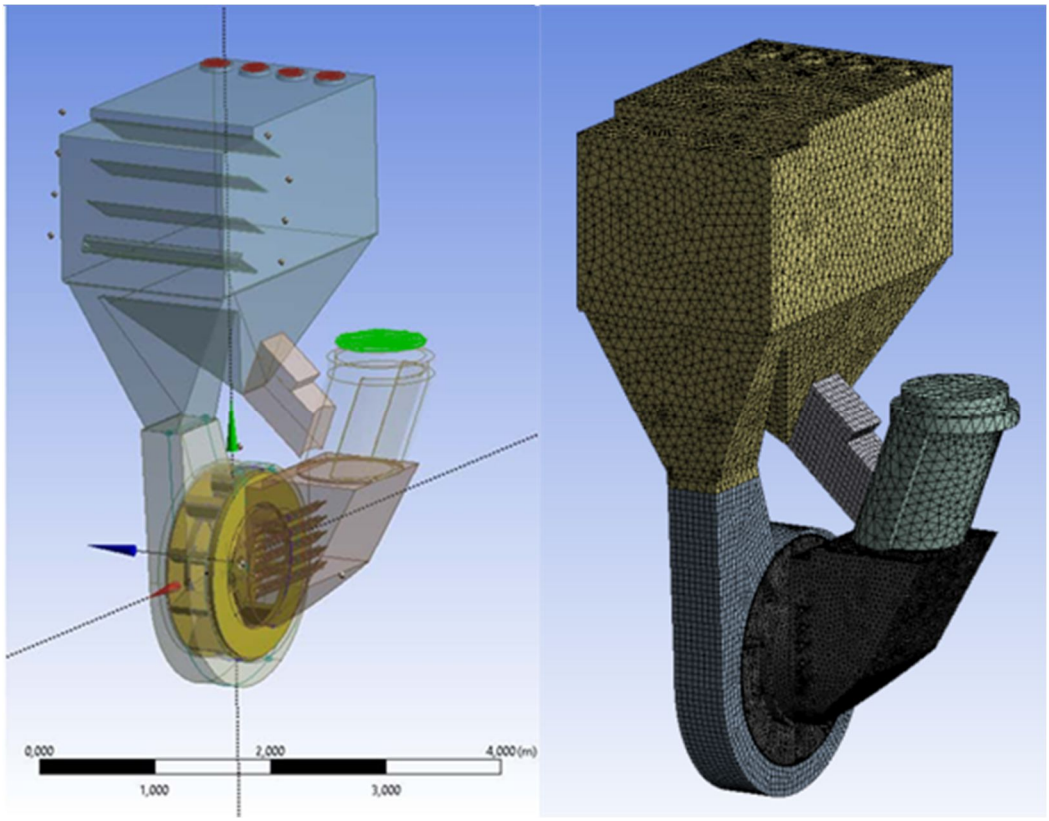

Figure 1. Geometry (left) and mesh (right) shown. Mesh consisted of approx. 600.000 elements.

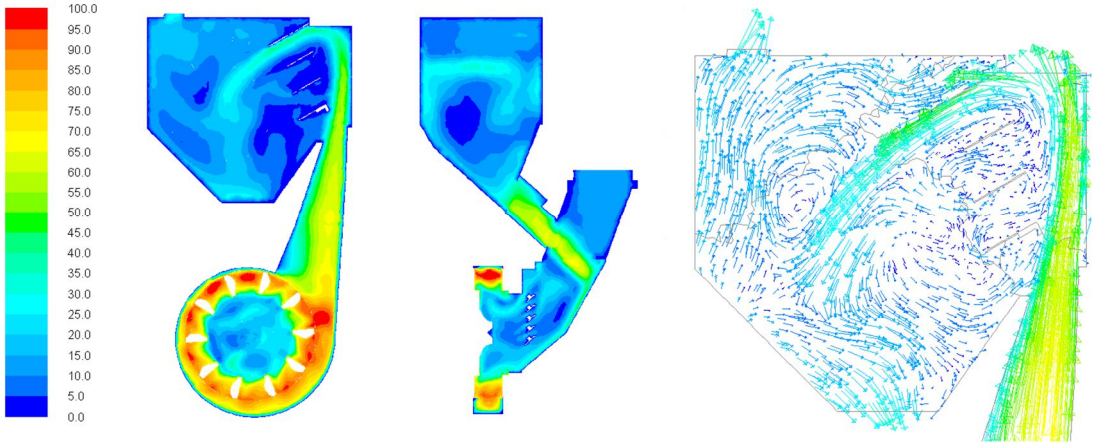

Figure 2. Velocity contours in 2 cross-sections (left) and velocity vectors in the classifier. Coloured by fluid velocity magnitude [m/s].

5. Obtained results

Figures 3-6 present the results obtained from 3 different perspectives; the side (figure 3), the back (figure 4 and 6) and from the top (figure 5). Each figure show the evolution of the particle movement in the mill with a 0.1 s interval. The first figure presents the particles 0.22 seconds after injection. The left side of each figure shows the smallest particles whilst the right side, the biggest. After 0.72 seconds the particles escaped from the domain were counted, these results are presented in figure 7 in the form of a line chart. The results show a dominance of small particles to stick towards the front of the mill (towards the inlet), while big particles stay towards the side. This can be observed in figure 3. After being shed into the classifier the smaller particles tend to change their direction swiftly with the fluid. The bigger particles hit the ceiling of the mill's classifier, after bouncing from it, they are shed upwind with the fluid or are bounced from the lower flaps into the classifier. This depletes those particles of momentum, which they slowly regain due to the fluid's velocity. This can be observed in figure 4.

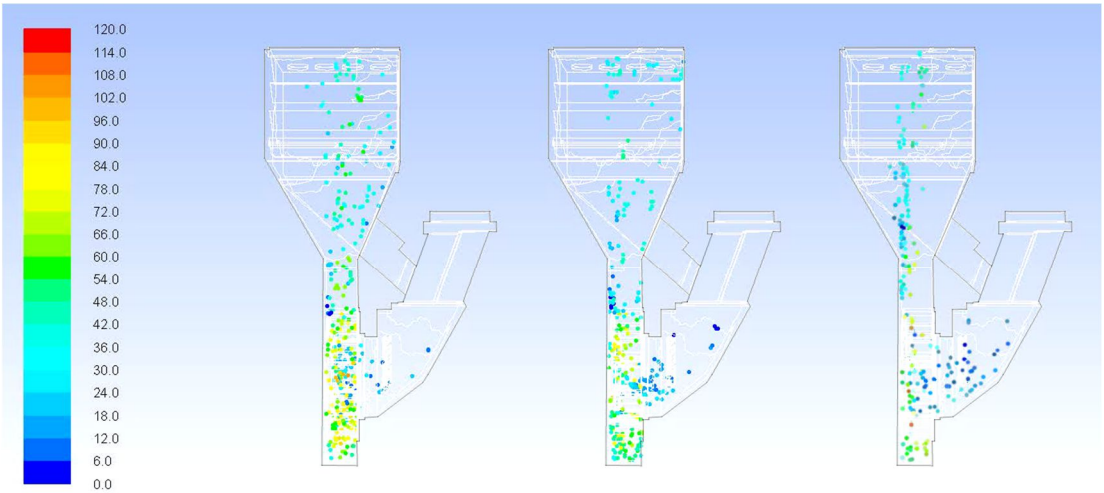

Figure 3. Particles coloured by particle velocity [m/s]. Particle diameter from left to right is appropriately; 10^{-6}, 10^{-5} and 10^{-4} m. Time step shown: 0.22 seconds after particle injection.

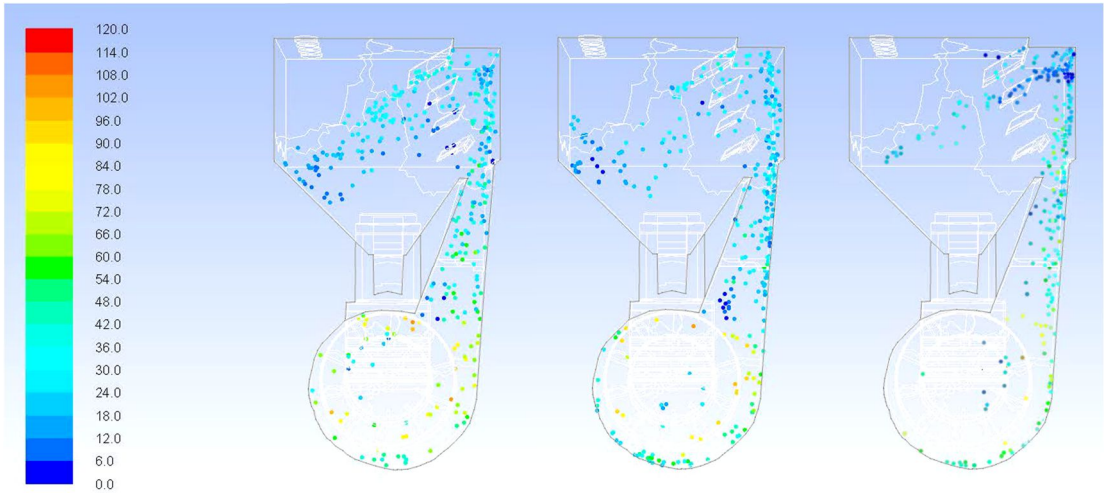

Figure 4. Particles coloured by particle velocity [m/s]. Particle diameter from left to right is appropriately; 10^{-6}, 10^{-5} and 10^{-4} m. Time step shown: 0.32 seconds after particle injection.

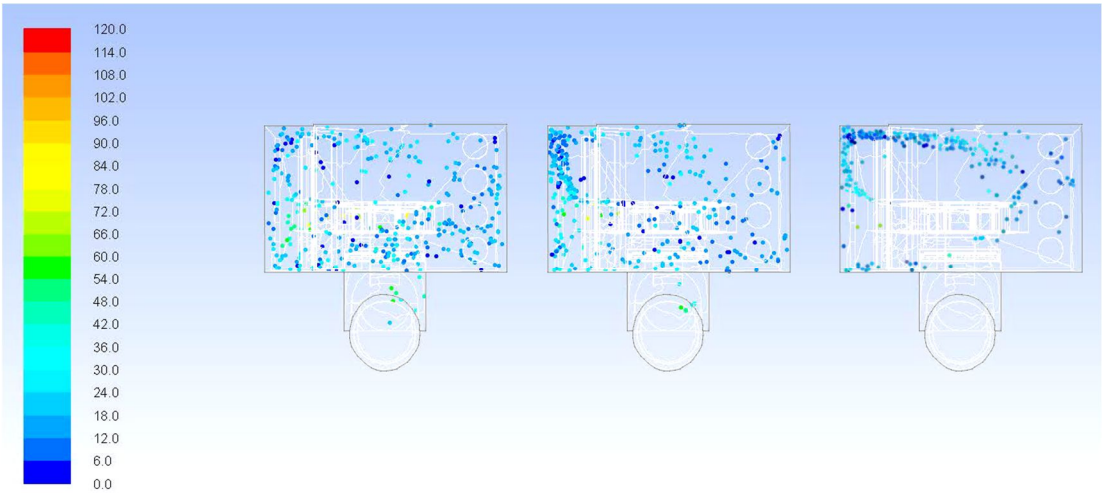

Figure 5. Particles coloured by particle velocity [m/s]. Particle diameter from left to right is appropriately; 10^{-6}, 10^{-5} and 10^{-4} m. Time step shown: 0.42 seconds after particle injection.

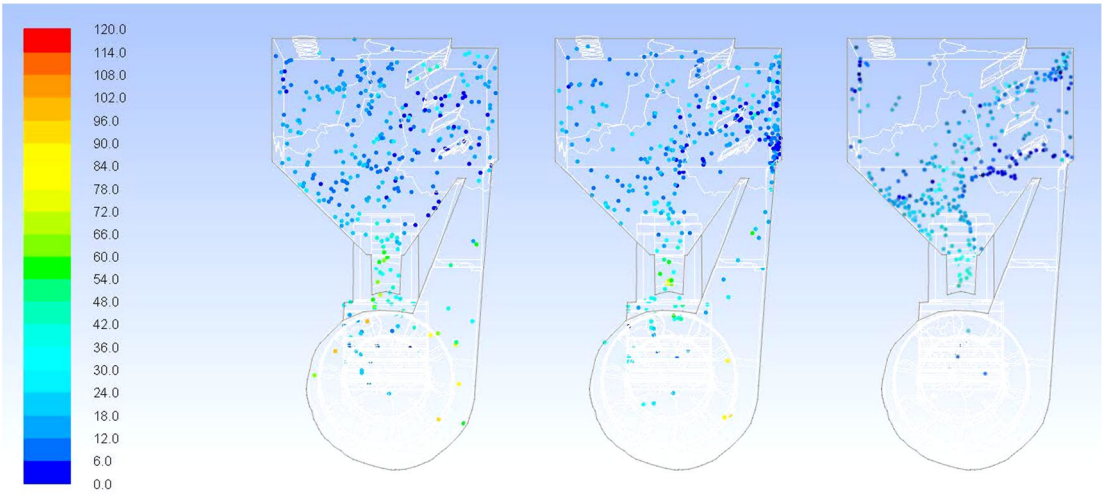

Figure 6. Particles coloured by particle velocity [m/s]. Particle diameter from left to right is appropriately; 10^{-6}, 10^{-5} and 10^{-4} m. Time step shown: 0.52 seconds after particle injection.

Figure 5 present a curvilinear motion of all the particles: after they are shed up they turn towards the injection side wall and start their descent towards the recirculation channel. This movement is found dominant for the biggest particles studied. In figure 6 we can observe an dominance for the biggest particles in the lower regions of the classifier (near the recirculation channel). This happens due to – after regaining momentum due to the fluid – the particles hit the oncoming wall of the classifier and lose their momentum. This happens for all the particles only the bigger particles are more affected due to a longer time needed to regain momentum in the surrounding fluid velocity field. In the following step gravity takes its toll and pulls them into the recirculation channel. Those particles were observed to recirculate the most, while the smallest particles remained suspended in the vortices of the classifier. This suspension would not occur for particles that remained near the wall. As can be seen in figure 2 the velocity vectors of the fluid near that region would drag the particles towards the outlet if they would stay near the wall. However they can get very easily caught in the stream leading them towards the suspension vortices. A change of outlet size and position could affect this behaviour and allow for better particle filtration. Moreover, clogging of particles of 10^{-5} m size has been observed

near the entry of the classifier. The widening of the stream seams to affect only particles of this size. The amount of escaped particles shown in figure 7 is surprisingly small but one has to keep in mind that this is a time period of 0.72 seconds. The shape of the plot is considered correct due to a higher percentile of smaller particles filtered.

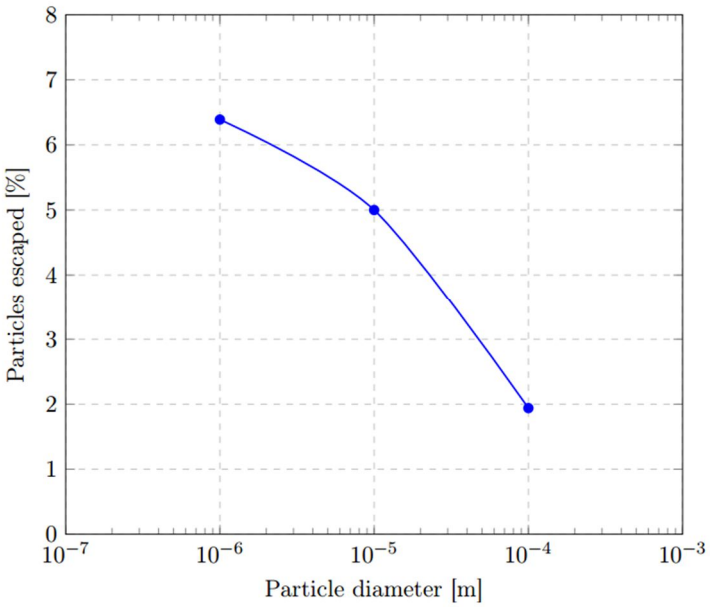

Figure 7. Particles escaped from domain in function of particle diameter after 0.72 seconds after injection.

6. Conclusions

We conducted a study of particle-fluid interaction inside a beater mil with the use of a CFD-DEM code. We chose 3 representative group sizes, which showed different behaviour. Upon analyses of the obtained data we concluded that the effectiveness of the mill can be increased by applying the following geometrical improvements:

- By creating a channel of fluid moving from the flaps towards the outlet at a high velocity. The presents of such a channel should provide a sufficient curvature to shed out the bigger particles, while retaining the smaller ones, thus improving the effectiveness of the classifier.
- The absence of large low-velocity vortices that would not allow the suspension of smaller particles. This can be achieved by compacting the classifier and changing the geometry to create a channel mentioned above.
- The 2 lower flaps of the classifier seem to have none effect on the fluid flow and can be with ease deleted or moved towards a place, where they can contradict the large low-velocity vortices. They do however bounce some of the larger particles inside the classifier's domain.
- The ceiling part of the classifier between the upper flap and the right side (while looking at figure 6) should be angled to allow the particles to bounce off from the wall towards the inside of the classifier, instead of clogging up this region.
- Additional clogging has been observed near the classifier entry surface. It seems to mostly affect particles of the 10^{-5} m size group.
- A change of position and/or size of the outlets should improve the filtration process.

Acknowledgment

The authors would like to acknowledge the financial support from the Polish NCBiR and KGHM granted upon the contract number CuBR/I/3/NCBR/2014.

References

[1] Cleary P W 1998 *Predicting charge motion, power draw, segregation and wear in ball mills using discrete element methods* Minerals Engineering 11 (11)
[2] Azimian M Lichti M and Bart H J 2014 *Investigation of particulate flow in a channel by application of CFD, DEM and LDAPDA* The Open Chemical Engineering Journal 8 1–11
[3] Yang C and Duan Y 2013 *CFD-DEM model for simulating solid exchange in a dual-leg fluidized bed* Chemical Engineering and Technology. 36 (11), 1907–1914
[4] Kubicki D and LO S 2012 *Slurry transport in a pipeline Comparison of CFD and DEM models* Ninth International Conference on CFD in the Minerals and Process Industries 10-12 December
[5] Kloss C Goniva C Hager A Amberger S and Pirker S 2012 *Models, algorithms and validation for opensource DEM and CFD-DEM* Progress in Computational Fluid Dynamics 12 (2/3) 140–152
[6] D C Wilcox 1998 *Turbulence Modelling for CFD* DCW Industries Inc. La Canada, California
[7] Cundall P A Stark O D 1979 *A discrete numerical model for granular assemblies* Géotechnique, 29, 47-65